A substrate of the ABC transporter PEN3 stimulates bacterial flagellin (flg22)-induced callose deposition in *Arabidopsis thaliana*

Andreas Matern[‡], Christoph Böttcher[‡1], Lennart Eschen-Lippold[‡], Bernhard Westermann[§], Ulrike Smolka[‡], Stefanie Döll[‡], Fabian Trempel[‡], Bibek Aryal[¶], Dierk Scheel[‡], Markus Geisler[¶], and Sabine Rosahl[‡2]

From the [‡]Department of Stress and Developmental Biology and [§]Department of Bioorganic Chemistry, Leibniz Institute of Plant Biochemistry, Weinberg 3, D-06120 Halle (Saale), Germany and the [¶]Department of Biology, University of Fribourg, Chemin du Musée 10, CH-1700 Fribourg, Switzerland

Nonhost resistance of *Arabidopsis thaliana* against *Phytophthora infestans*, a filamentous eukaryotic microbe and the causal agent of potato late blight, is based on a multilayered defense system. *Arabidopsis thaliana* controls pathogen entry through the penetration-resistance genes *PEN2* and *PEN3*, encoding an atypical myrosinase and an ABC transporter, respectively, required for synthesis and export of unknown indole compounds. To identify pathogen-elicited leaf surface metabolites and further unravel nonhost resistance in *Arabidopsis*, we performed untargeted metabolite profiling by incubating a *P. infestans* zoospore suspension on leaves of WT or *pen3* mutant *Arabidopsis* plants. Among the plant-secreted metabolites, 4-methoxyindol-3-yl-methanol and *S*-(4-methoxy-indol-3-yl-methyl) cysteine were detected in spore suspensions recollected from WT plants, but at reduced levels from the *pen3* mutant plants. In both whole-cell and microsome-based assays, 4-methoxyindol-3-yl-methanol was transported in a PEN3-dependent manner, suggesting that this compound is a PEN3 substrate. The syntheses of both compounds were dependent on functional PEN2 and phytochelatin synthase 1. None of these compounds inhibited mycelial growth of *P. infestans in vitro*. Of note, exogenous application of 4-methoxyindol-3-yl methanol slightly elevated cytosolic Ca^{2+} levels and enhanced callose deposition in hydathodes of seedlings treated with a bacterial pathogen-associated molecular pattern (PAMP), flagellin (flg22). Loss of flg22-induced callose deposition in leaves of *pen3* seedlings was partially reverted by the addition of 4-methoxyindol-3-yl methanol. In conclusion, we have identified a specific indole compound that is a substrate for PEN3 and contributes to the plant defense response against microbial pathogens.

Phytophthora infestans is the causal agent of late blight, economically the most important potato disease. In an attempt to understand resistance against infection by this oomycete, attention has turned to nonhost pathosystems, such as the interaction of *Arabidopsis thaliana* and *P. infestans* (1). Nonhost resistance involves multiple layers of defense, including pre- and postinvasion resistance (2). In addition to constitutive barriers, induced defense mechanisms contribute to nonhost resistance, which are activated in the plant upon recognition of pathogen-associated molecular patterns (PAMPs)[3] (3). Moreover, recognition of pathogen effectors, which suppress plant immunity, by plant resistance gene products has an impact on nonhost resistance in a number of pathosystems (2). The relative contribution of PAMP-triggered immunity or effector-triggered immunity to nonhost resistance differs according to the evolutionary distance of host and nonhost plants (4).

The identification of *penetration* (*pen*) mutants in genetic screens with the nonadapted barley pathogen *Blumeria graminis* f.sp. *hordei* (*Bgh*) provided the first insights into defense strategies at the cell periphery in the nonhost resistance response. *PEN2* encodes a myrosinase that catalyzes the degradation of indole glucosinolates (IGs) (5–7). Products of the PEN2 reaction are postulated to be transported to the apoplast by the ABC transporter PEN3/ABCG36/PDR8 (hereafter referred to as PEN3) (8). Loss of PEN2 or PEN3 function results in enhanced penetration of nonadapted filamentous pathogens (5, 8, 9), emphasizing the importance of defense at the cell periphery for pathogen entry control.

Glucosinolates are secondary metabolites specific for the order *Capparales* and act as insect deterrents. As phytoanticipins, IGs accumulate constitutively in plant tissue and are synthesized from tryptophan with indol-3-ylacetaldoxime

[3] The abbreviations used are: PAMP, pathogen-associated molecular pattern; IAN, indoleacetonitrile; *Bgh*, *Blumeria graminis* f.sp. *hordei*; Cys(IAN), cysteine-indole-3-acetonitrile conjugate; DHCA, dihydrocamalexic acid; I3CHO, indole-3-carbaldehyde; I3COOH, indole-3-carboxylic acid; 1MeI3COOH, 1-methyl indole-3-carboxylic acid; I3COOMe, indole-3-carboxyl-methyl ester; I3G, indol-3-ylmethyl glucosinolate; I3MA, indol-3-yl-methyl amine; 4MeOI3G, 4-methoxyindol-3-yl methyl glucosinolate; 4MeOI3M, 4-methoxyindole-3-methanol; 4MeOI3Cys, *S*-(4-methoxy-indol-3-ylmethyl) cysteine; IG, indole glucosinolate; 4GlcOI3F, 4-β-D-glucosyloxy-indol-3-yl formamide; 4OHI3CHO, 4-hydroxyindole-3-carbaldehyde; IBA, indole butyric acid; IAA, indole-3 acetic acid; CID, collision-induced dissociation; MAPK, mitogen-activated protein kinase; ESI, electrospray ionization.

Table 1

Analytical data of compounds detected by UPLC/ESI-QTOF MS in *P. infestans* spore suspension recollected after 24 h from *A. thaliana* WT leaves

Confidence level of annotation (according to Ref. 51) is as follows: 1, verified with mass, retention time, and CID spectrum of a commercial standard or a synthesized standard (*); 2, putatively annotated compounds based on CID spectrum interpretation, data base hits, and literature.

Annotation	Elemental composition	Retention time	Quantifier ion				Annotation level
		min	Type	*m/z*	Type	*m/z*	
Camalexin	$C_{11}H_8N_2S$	6.6	$[M + H]^+$	201.0481	$[M - H]^-$	199.0335	1
Dihydrocamalexic acid (DHCA)	$C_{12}H_{10}N_2O_2S$	3.8	$[M + H]^+$	247.0536	$[M - H]^-$	245.0390	1*
2-Foramidophenyl-2′-thiazolylketone	$C_{11}H_8N_2O_2S$	6.0	$[M + H]^+$	233.0379			1*
Indol-3-ylmethyl amine (I3MA)	$C_9H_{10}N_2$	1.9	$[M + H-NH_3]^+$	130.0651			1
Indol-3-carboxylic acid (I3COOH)	$C_9H_7NO_2$	4.7	$[M + H]^+$	162.0550	$[M - H]^-$	160.0404	1
Methyl indole-3-carboxylate (I3COOMe)	$C_{10}H_9NO_2$	6.6			$[M - H]^-$	174.056	1
1-Methyl-indole-3-carboxylic acid (1MeI3COOH)	$C_{10}H_9NO_2$	5.9	$[M + H]^+$	176.0706			1
Indole-3-carbaldehyde (I3CHO)	C_9H_7NO	4.8	$[M + H]^+$	146.0600	$[M - H]^-$	144.0450	1
4-Hydroxyindole-3-carbaldehyde (4OHI3CHO)	$C_9H_7NO_2$	5.1	$[M + H]^+$	162.0550	$[M - H]^-$	160.0404	1
p-Coumaroylagmatine (*cis/trans*)	$C_{14}H_{20}N_4O_2$	2.9/3.3	$[M + H]^+$	277.1659			1
Kaempferol 3,7-di-*O*-α-Rha (K 3,7-Rha$_2$)	$C_{27}H_{30}O_{14}$	4.7	$[M + H]^+$	579.1708	$[M - H]^-$	577.1562	2
Kaempferol 3-*O*-β-Glc-7-*O*-α-Rha (K 3-Glc-7-Rha)	$C_{27}H_{30}O_{15}$	4.3	$[M + H]^+$	595.1658	$[M - H]^-$	593.1511	2
Sinapoylmalate	$C_{15}H_{16}O_9$	4.6	$[M + H - C_4H_6O_5]^+$	207.0652	$[M - H]^-$	339.0720	2
Scopoletin	$C_{10}H_8O_4$	4.5	$[M + H]^+$	193.0495	$[M - H]^-$	191.0350	1
S-(4-Methoxyindol-3-ylmethyl)cysteine	$C_{13}H_{17}N_2O_3S$	4.2	$[M + H]^+$	281.09			1*
4-Methoxyindol-3-ylmethanol	$C_{10}H_{11}NO_2$	5.0	$[M + Na]^+$	200.06			1*
8-Methylsulphinyloctyl (NHCOSMe)	$C_{11}H_{23}NO_2S_2$	5.9	$[M + Na]^+$	288.1062		-	2
Leucyl-proline (H-Leu-Pro-OH)	$C_{11}H_{20}N_2O_3$	2.5	$[M + H]^+$	229.1546	$[M - H]^-$	227.1390	1*

and indole-3-ylacetothiohydroximic acid as intermediates (reviewed in Ref. 10). Modifications of the indole ring such as hydroxylation and subsequent methylation, leading to the formation of 4-hydroxyindol-3-ylmethyl glucosinolate (4OHI3G) and 4-methoxyindol-3-ylmethyl glucosinolate (4MeOI3G), respectively, require the enzymes CYP81F2 and the indole glucosinolate *O*-methyltransferases IGMT1 or IGMT2 (11). Whereas heterologously expressed PEN2 protein cleaves both indol-3-ylmethyl glucosinolate (I3G) and 4MeOI3G *in vitro*, mutant analyses point to the importance of 4MeOI3G-derived metabolites for pathogen defense (6). Recently, the GSH-*S*-transferase GSTU13 was shown to be required for PEN2-dependent metabolism of IGs, with preference for 4-*O*-substituted IGs (12).

The observation that *pen2* and *pen3* mutants are also impaired in callose formation in response to treatment with the bacterial PAMP flg22 suggested that a PEN2 product, exported by the transporter PEN3, acts as a signaling molecule or a coactivator (7). On the other hand, it has been hypothesized that the compounds exported by PEN3 have toxicity to invading pathogens (8, 13, 14).

In search for small molecules that are transported by PEN3, indole compounds hyperaccumulating in *pen3* mutant plants inoculated with *Bgh* have been identified. In addition to the PEN2 substrate 4MeOI3G (6, 7), 4-β-D-glucosyloxy-indol-3-yl formamide (4GlcOI3F) accumulated in several mutants with different *pen3* alleles (15). Here, we report the identification of two novel indole derivatives from the surface of *P. infestans*-inoculated *Arabidopsis* plants, which are present at significantly lower levels on *pen3* plants. None of the compounds inhibited mycelial growth of *P. infestans in vitro*. Rather, the ability of 4-methoxyindole-3-methanol (4MeOI3M) to enhance flg22-induced callose formation suggests that this PEN3-dependently exported compound acts as a modulator of defense.

Results

Identification of secondary metabolites accumulating extracellularly in response to *P. infestans* inoculation

To assess the extent of extracellular chemical defense in the nonhost resistance response of *Arabidopsis* to *P. infestans* infection, untargeted metabolite profiling was performed. Leaves of Col-0 *Arabidopsis* plants were drop-inoculated with water or a *P. infestans* zoospore suspension. The inoculum was removed after 24 h, concentrated, dissolved in 30% methanol, and subjected to UPLC-ESI-QTOF-MS (16). Comparative analyses of the metabolic profiles revealed the presence of more than 1000 features significantly increased in zoospore suspension droplets recollected from Col-0 plants compared with the control. Up to 25% of these features could also be detected in a spore suspension without contact to plant leaves. Some of the spore suspension–derived compounds were tentatively annotated using an in-house analyte list as metabolites from the primary metabolism (sugars, phosphosugars, organic acids, amino acids, polyamines, purine derivatives and degradation products, and pipecolic acid (Table S1)). They could originate from the germinating spores, but also from the medium used for *P. infestans* cultivation. From the exclusively plant-derived features significantly increased in the treatment group, 18 recurring features could be annotated by accurate tandem MS analyses (Table 1 and Fig. 2A).

The extracellular occurrence of camalexin, 2-formamidophenyl-2′-thiazolylketone, and two unknown camalexin compounds was reported before (16). These compounds accumulated in a PAD3 (phytoalexin-deficient 3)-dependent manner (16). Here, additional compounds were detected and identified, which accumulated in *P. infestans* droplets but not in water controls (Table 1). Among these was the hydroxycinnamic acid amide coumaroylagmatine, exported by the MATE transporter DTX18 (17). In addition, indolic compounds, such as indol-3-ylmethyl amine (I3MA), indole-3-carbaldehyde (I3CHO), indole-3-carboxylic acid (I3COOH), indole-3-carboxyl-methyl ester (I3COOMe), 1-methyl indole-3-carboxylic acid (1MeI3COOH) and 4-hydroxy-
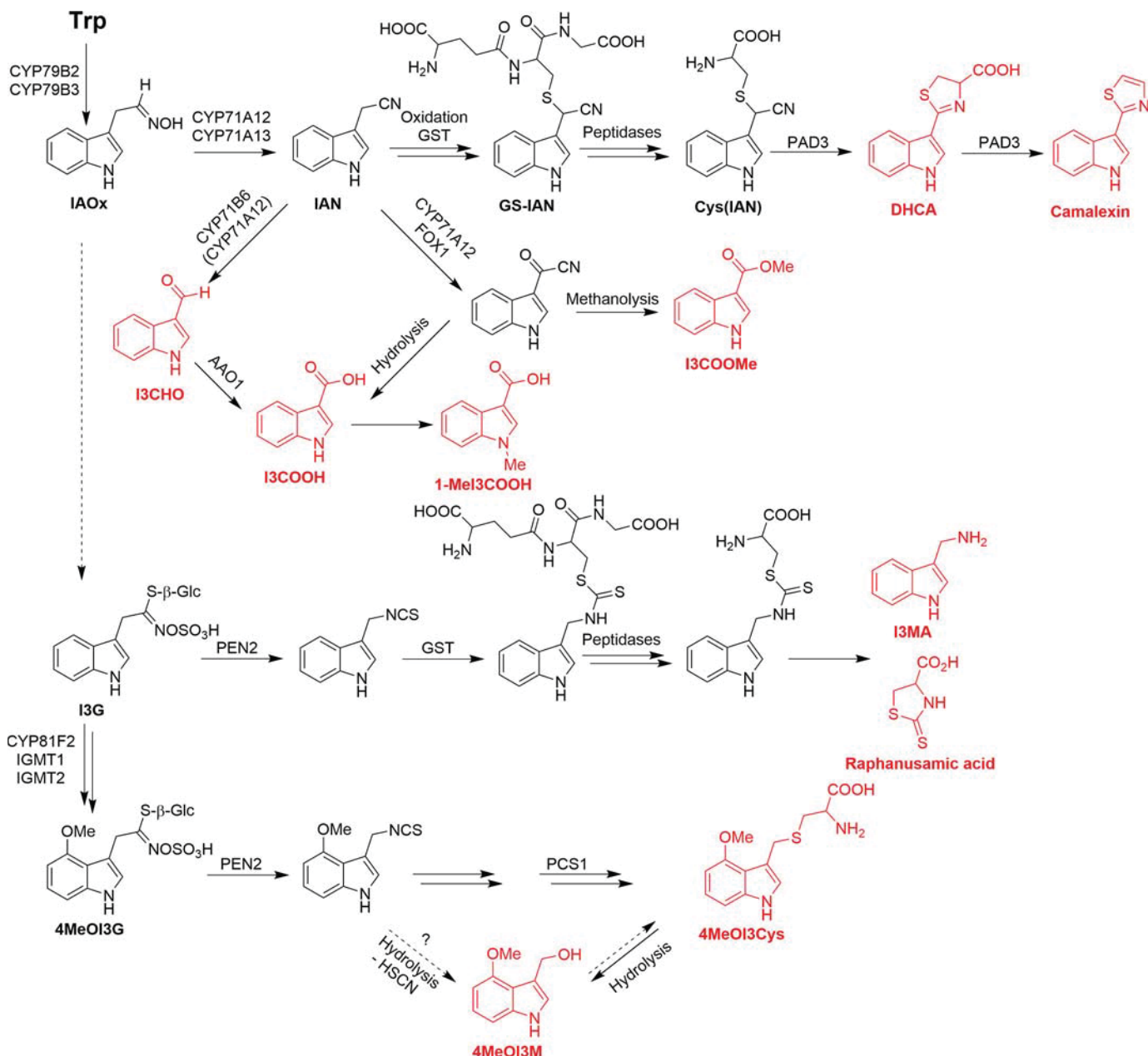
Figure 1. Proposed pathway leading to the *P. infestans*-induced formation of indole derivatives in *Arabidopsis*. Indole compounds analyzed in this study are indicated in *red*. *IAOx*, indole-3-acetaldoxime; *GS-IAN*, GSH-indole-3-acetonitrile.

indole-3-carbaldehyde (4OHI3CHO) were detectable. Importantly, two novel compounds were identified as substances exported in response to *P. infestans* challenge (Table 1). Based on comparison of chromatographic and mass spectral properties (Fig. S1) with synthetic standards that have been authenticated by ^{1}H and ^{13}C NMR, these were identified as *S*-(4-methoxy-indol-3-yl-methyl) cysteine (4MeOI3Cys) and 4MeOI3M.

A hypothetical pathway leading to the synthesis of the various indole compounds (Fig. 1) was generated based on data from the literature (6, 7, 16, 18, 19). Central to the synthesis of camalexin, as well as I3CHO and I3COOH, is indoleacetonitrile (IAN), which is formed from tryptophan through the action of CYP79B2/B3 and CYP71A13 (20). As proposed by Böttcher *et al.* (16), camalexin synthesis proceeds via oxidation of IAN followed by the addition of GSH to IAN, possibly by a GSH-*S*-

transferase, and removal of glycine and glutamic acid by peptidases or GSH γ-glutamylcysteinyltransferase 1 (CAD1, PCS1) to yield Cys(IAN), which is converted by CYP71B15 (PAD3) to dihydrocamalexic acid (DHCA) and camalexin. IAN is also one possible precursor for I3CHO and I3COOH, which are synthesized by CYP71B6/CYP71A12 and AAO1 (18) or CYP71A12 and FOX1 followed by hydrolysis or, for I3COOMe, methanolysis during sample preparation (19).

Indole compounds derived from the PEN2 pathway are degradation products of indole glucosinolates. PEN2 has been shown to cleave both I3G and 4MeOI3G *in vitro* (6). The newly discovered compounds 4MeOI3Cys and 4MeOI3M are hypothesized to be derived from the primary PEN2 product, 4-methoxyindol-3-ylmethyl isothiocyanate. Due to its reactivity, this isothiocyanate can be directly hydrolyzed to give

4MeOI3M or, by yet unidentified enzymes, converted to 4MeOI3Cys. Because the *pcs1* mutant *cad1-3* shows enhanced penetration of *P. infestans* (21), involvement of the phytochelatin synthase 1 (PCS1) in proteolytic processing of an intermediate can be hypothesized.

Identification of secondary metabolites accumulating extracellularly in response to P. infestans inoculation in a PEN3-dependent manner

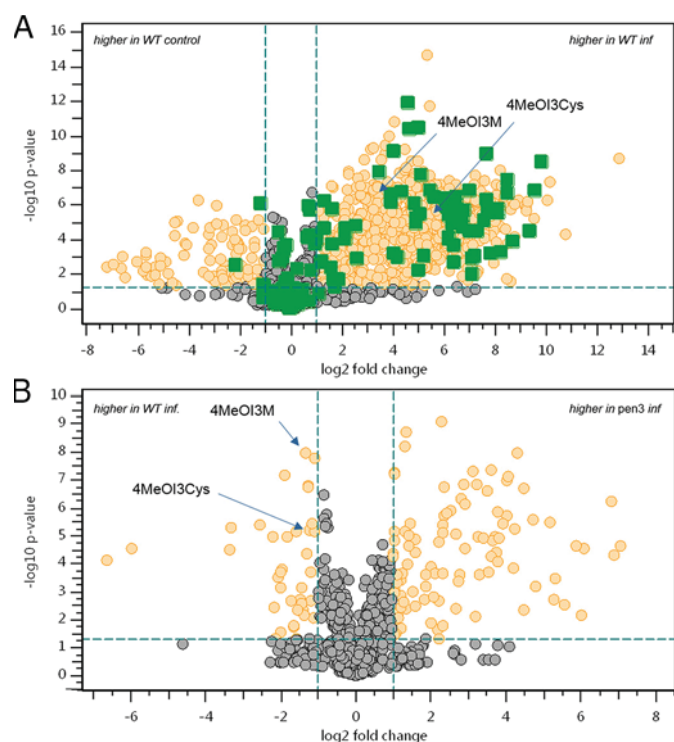To identify PEN2-derived metabolites that accumulate extracellularly in a PEN3-dependent manner, untargeted

Figure 2. Untargeted metabolite profiling with droplets containing a *P. infestans* spore suspension applied on the leaf surface of *A. thaliana*. Droplets were collected after 24 h of incubation. *A*, WT treatment *versus* control. *Volcano plot*, visualization of 2039 single *t* test results for each detected feature in the data set (*gray*, *green*, and *yellow dots*; n = 6). Additionally, a spore suspension without leaf contact was measured. Features that were also detected in the spore suspension are *colored* in *green*. *Yellow dots*, features significantly different with $p < 0.05$ and a -fold change ≥ 2. *B*, visualization of *t* test results from the comparison of infected WT (*WT inf*; n = 6) *versus* infected *pen3* (*pen3 inf*; n = 9). Data are derived from one experiment representative of four independent experiments.

metabolite profiling was performed using *P. infestans*-inoculated *pen2-1* mutant plants and the respective WT *gl1*, as well as *pen3-1* (8) and *cad1-3* (22) (*pcs1*) plants and their WT Col-0. Metabolite profiling was performed of the inoculum incubated on leaves for 24 h and of methanolic extracts of the infected leaf tissue below the inoculum, to detect extracellular and tissue-associated metabolites, respectively. For each feature delivered by the peak picking algorithm, a Student's *t* test was calculated comparing each mutant to its respective WT. Several compounds increased more than 2-fold in the mutants (Fig. 2*B* and Table S2), whereas the number of features with a significantly higher accumulation in the WT, which may comprise the PEN3 substrates, was very low (Fig. 2*B*).

To avoid false positive results, only features were considered that differentially accumulated in the same manner throughout several experimental repetitions. For the potential PEN3 substrates, these were only seven metabolites (Table 2).

Candidates for possible PEN3 substrates and further identified compounds involved in the defense against *P. infestans* (Tables 1 and 2) were quantified in targeted LC-MS analyses in WTs and mutants. Both intra- and extracellularly, camalexin was present in significantly higher amounts in all mutants analyzed, *pen3-1*, *cad1-3*, and *pen2-1*, compared with their respective WTs (Figs. 3 and S2). DHCA levels were also enhanced in methanolic extracts of *pen3-1*, *cad1-3*, and *pen2-1* and in the inoculum of *cad1-3* and *pen2-1*, but not *pen3-1* (Figs. 3 and S2).

There were no differences in the levels of I3G (data not shown). I3CHO was present at very low amounts in methanolic extracts of *P. infestans*-inoculated leaves of all lines analyzed (Figs. 3*A* and S2*A*). In contrast, extracellular levels of I3CHO were significantly reduced in *pen3-1* but not in *cad1-3* and *pen2-1* plants (Figs. 3*B* and S2*B*). Enhanced levels of I3COOH were detected in all mutant leaves. Extracellular levels were drastically enhanced in *cad1-3* and *pen2-1* plants, but not significantly different in *pen3-1* and WT plants. These observations do not suggest a clear dependence of synthesis and secretion of I3CHO and I3COOH on *PEN* genes.

The reduced levels of I3MA and raphanusamic acid in *pen2-1* plants suggested that these compounds are downstream products of the PEN2-mediated reaction (6). In accordance with this, *P. infestans*-infected leaves of *cad1-3* and *pen2-1* plants contain lower levels of these substances (Figs. 3*A* and S2*A*). Moreover, I3MA was not detectable in the inoculum col-

Table 2

Compounds detected by UPLC/ESI-QTOF MS in *P. infestans* spore suspension recollected after 24 h from *A. thaliana* leaves, which were significantly increased in WT compared with *pen3*

Confidence level of annotation (according to Ref. 51) is as follows: 1, verified with mass, retention time, and CID spectrum of a commercial standard or a synthesized standard (*); 3, putative compound class, based on similarity of in-source fragmentation and CID spectrum to known compound classes.

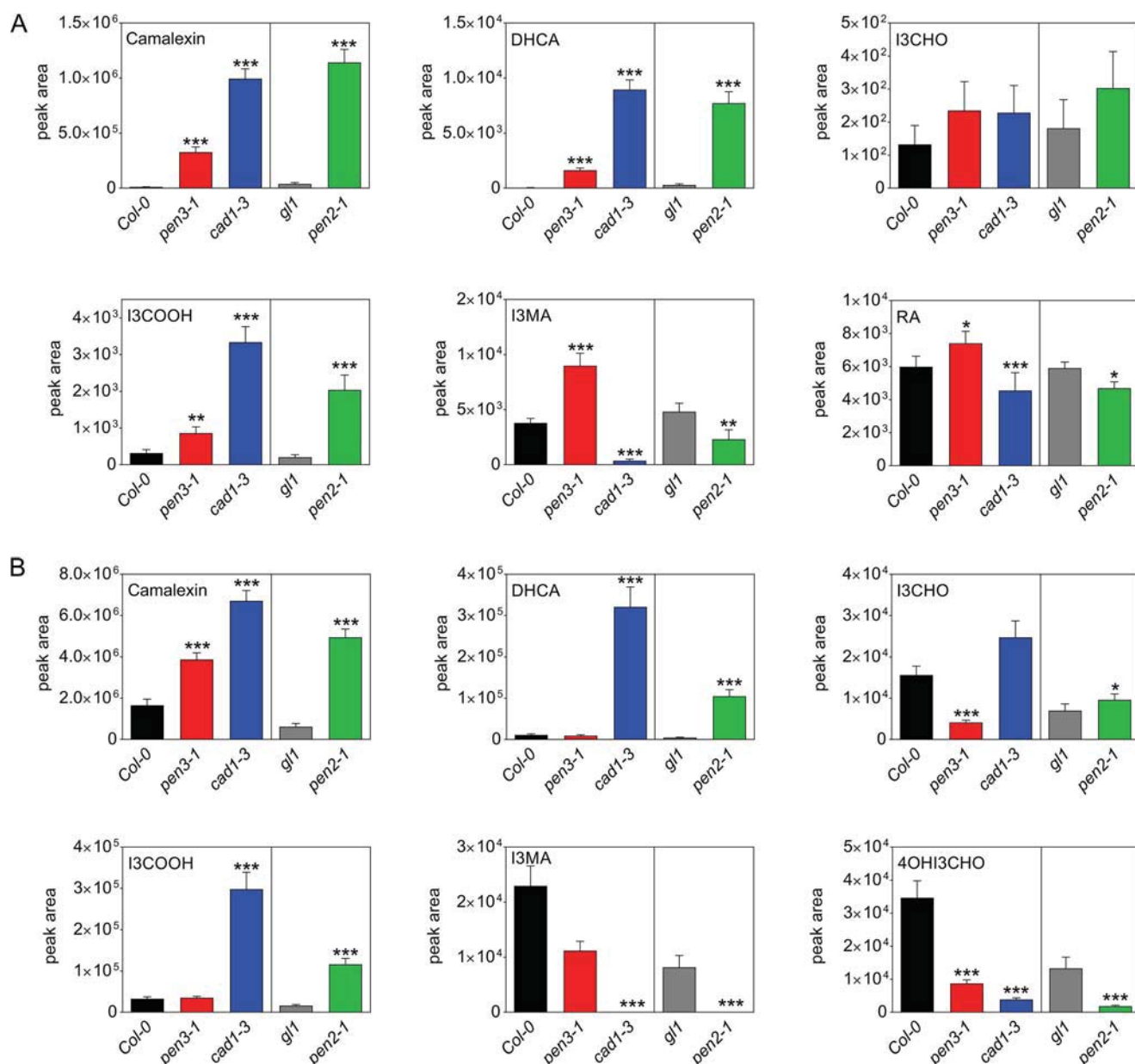| Annotation	Elemental composition	Retention time	Change *pen3*/Col-0	Quantifier ion *m/z* type	Quantifier ion *m/z*	Annotation level	Present in *pen2*
		min	*-fold*				
(E)-p-Coumaroylagmatine	$C_{14}H_{20}N_4O_2$	3.3	−9.6	$[M + H]^+$	277.16547	1*	Reduced
S-(4-Methoxyindol-3-ylmethyl) cysteine	$C_{13}H_{17}N_2O_3S$	4.22	−3.2	$[M + H]^+$	281.0942	1*	No
4-Methoxyindol-3-yl methanol	$C_{10}H_{11}NO_2$	5.03	−3.7	$[M + H]^+$	160.07499	1*	No
4-Hydroxyindole-3-carbaldehyde (4OHI3CHO)	$C_9H_7NO_2$	5.1	−3.0	$[M + H]^+$	162.05519	1	No
Unknown indole 1	$C_{10}H_9NO_2$	5.57	−2.5	$[M + H]^+$	176.07116	3	No
Unknown indole 2	$C_{10}H_9NO$	6.01	−4.1	$[M + H]^+$	160.07534	3	No
Unknown indole 3	$C_{10}H_9NO_2$	6.68	−3.6	$[M + H]^+$	176.07054	3	Reduced

Figure 3. Intracellular and extracellular levels of indol-3-ylmethyl glucosinolate–derived compounds in *P. infestans*-inoculated *Arabidopsis* leaves.
Leaves of the *Arabidopsis* mutants *pen3-1* (*red bars*), *cad1-3* (*blue bars*), and *pen2-1* (*green bars*), as well as their respective WTs Col-0 (*black bars*) and *gl1* (*gray bars*) were drop-inoculated with a *P. infestans* zoospore suspension (5×10^5 spores ml^{-1}). The inoculum and the leaf areas *below* the inoculation sites were collected separately after 24 h. Metabolite levels were determined by UPLC-ESI-QTOF-MS in methanolic extracts of inoculation sites (*A*) and in the inoculum (*B*). Data are derived from at least three independent experiments ($n \geq 15$). *Error bars*, S.E. Significance analyses were performed using Mann-Whitney two-tailed *U* test (mutant *versus* respective WT; *, $p < 0.05$; **, $p < 0.01$; ***, $p < 0.001$). RA, raphanusamic acid.

lected from *cad1-3* and *pen2-1* leaves. However, in *P. infestans* inoculum collected from *pen3-1* plants, I3MA levels were not significantly different from those on Col-0 plants, suggesting that the export of I3MA to the apoplast is independent of PEN3. Thus, there is no correlation between decreased I3MA levels and the phenotype of enhanced penetration, which is observed in *pen2-1*, *cad1-3*, and *pen3-1* plants.

Compounds accumulating on the leaf surface in a PEN2-, PCS1-, and PEN3-dependent manner included 4OHI3CHO (Figs. 3*B* and S2*B*) and three unidentified indole compounds (Table 2). These compounds might possibly be substrates of the ABC transporter PEN3. In addition, two compounds derived from 4MeOI3G, 4MeOI3Cys and 4MeOI3M, were identified as

metabolites that accumulated in the inoculum of WT, but not of *pen2-1*, *cad1-3*, or *pen3-1* plants. In methanolic extracts, both compounds were present at very low and variable amounts, whereas their precursor, 4MeOI3G, accumulated to higher levels in mutant compared with WT leaves (Figs. 4*A* and S3*A*). Extracellular levels of both 4MeOI3Cys and 4MeOI3M were highly reduced in all three mutants compared with the respective WTs (Figs. 4*B* and S3*B*). Moreover, decreased levels of both compounds were observed on the surface of two additional mutants, *pen3-3* and *pen3-4* (Figs. 4*C* and S3*C*).

The highly decreased levels of 4MeOI3Cys and 4MeOI3M in *pen2-1* and *cad1-3* mutants indicate that the encoded enzymes are required for the synthesis of these compounds. Importantly, the
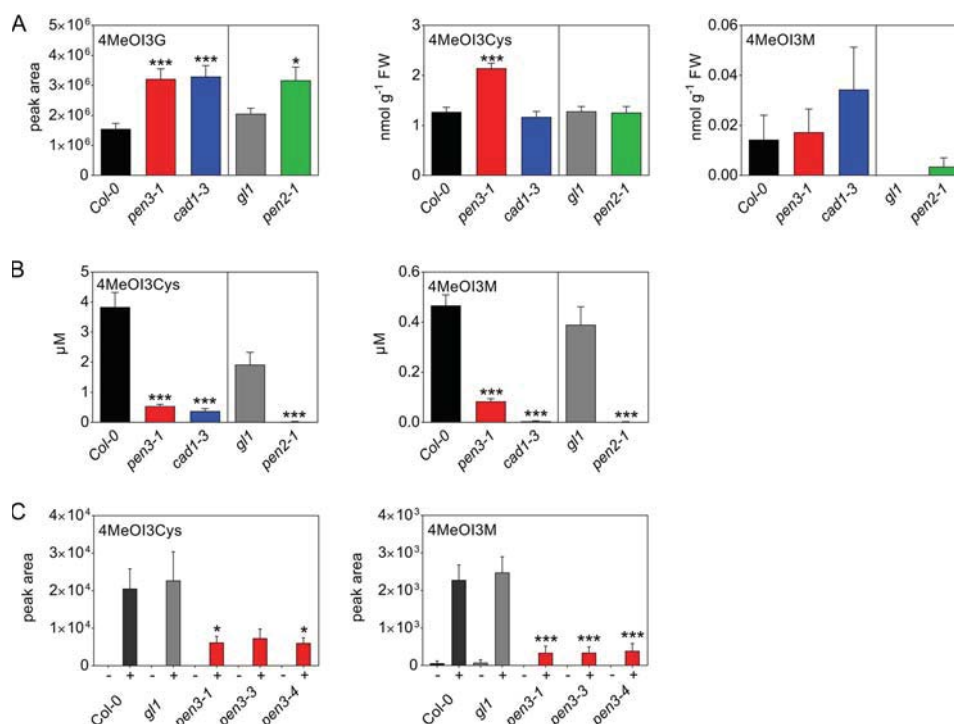
Figure 4. Intracellular and extracellular levels of 4MeOI3G-derived compounds in *P. infestans*-inoculated *Arabidopsis* leaves. Leaves of the *Arabidopsis* mutants *pen3-1* (*red bars*), *cad1-3* (*blue bars*), and *pen2-1* (*green bars*), as well as their respective WTs Col-0 (*black bars*) and *gl1* (*gray bars*), were drop-inoculated with a *P. infestans* zoospore suspension (5×10^5 spores ml^{-1}). The inoculum and the leaf areas below the inoculation sites were collected separately after 24 h. Metabolite levels were determined by UPLC-ESI-QTOF-MS in methanolic extracts of inoculation sites (*A*) and in the inoculum (*B*). Data are derived from at least three independent experiments ($n \geq 15$). *C*, metabolite levels were determined in the inoculum ($-$, water; $+$, *P. infestans*) from Col-0 (*black bars*), *gl1* (*gray bars*), *pen3-1*, *pen3-3*, and *pen3-4* (*red bars*) plants. Data are derived from three independent experiments ($n \geq 6$). *Error bars*, S.E. Significance analyses were performed using the Mann–Whitney two-tailed *U* test (mutant *versus* respective WT; *, $p < 0.05$; **, $p < 0.01$; ***, $p < 0.001$).

significantly reduced levels of 4MeOI3Cys and 4MeOI3M in the inoculum of *pen3* mutants suggest a requirement of a functional PEN3 transporter for the export of these compounds.

4MeOI3M is transported in a PEN3-dependent manner

Based on previous work it was suggested that PEN3/ABCG36/PDR8, like its close homolog PIS1/ABCG37/PDR9 (23), apparently has a wider substrate specificity toward a few structurally unrelated substrates (15, 24, 25). These include indole compounds (such as indole butyric acid (IBA)), although convincing transport data for PEN3 were only provided for cadmium (24). Direct transport analyses were performed using custom-synthesized, radiolabeled 4MeOI3M as a substrate. In single-cell transport assays using protoplasts prepared from transgenic *Arabidopsis* leaf material, constitutive overexpression of PEN3 led to significantly enhanced 4MeOI3M export, whereas loss of PEN3 function in *pen3-1* did not result in significantly reduced export (Fig. 5*A*). As expected, export of closely related indole-3 acetic acid (IAA), quantified in parallel in double-labeling assays, was not affected by the presence of PEN3 as was already shown for ABCG37 (23). Microsome-based transport assays verified whole-cell assays; both loss and gain of PEN3 function resulted in significantly reduced and enhanced 4MeOI3M uptake, respectively, whereas again IAA transport was not significantly disturbed (Fig. 5*B*). In the absence of ATP, uptake of 4MeOI3M by microsomes from PEN3-overexpressing but not from *pen3-4* plants was significantly reduced, as would be

expected for an ATP-driven transport catalyzed by an ABC transporter (Fig. 5*B*). Importantly, in competition experiments, uptake of radioactively labeled 4MeOI3M into PEN3-overexpressing microsomes was significantly inhibited in the presence of an excess of unlabeled 4MeIO3M and 4MeOI3Cys (Fig. 5*C*). In summary, direct transport and competition data support the conclusion that 4MeOI3M, and likely also 4MeOI3Cys, are PEN3 substrates.

4MeOI3Cys and 4MeOI3M are exported early after *P. infestans* inoculation

To elucidate the kinetics of export of specific compounds, time course experiments were performed with the *P. infestans* inoculum incubated on the surface of leaves of WT and mutant plants. Camalexin and DHCA started to accumulate between 4 and 6 h, with the highest levels in *pen2-1* and *cad1-3* (Fig. 6). The accumulation of I3CHO between 2 and 4 h after inoculation was similar in all plant lines analyzed, whereas I3COOH accumulation occurred later and was more pronounced in *pen2-1* and *cad1-3*. I3MA was not detectable in the biosynthesis mutants *pen2-1* and *cad1-3*, but it started to accumulate extracellularly in the WTs and in *pen3-1* 4 h postinoculation. 4MeOI3M and 4MeOI3Cys were hardly detectable in the inoculum incubated for 2 h, but their levels were significantly increased after 4 h in WT plants (Fig. 6). Thus, 4MeOI3M, 4MeOI3Cys, I3MA, and I3CHO are exported earlier than camalexin, DHCA, and I3COOH.
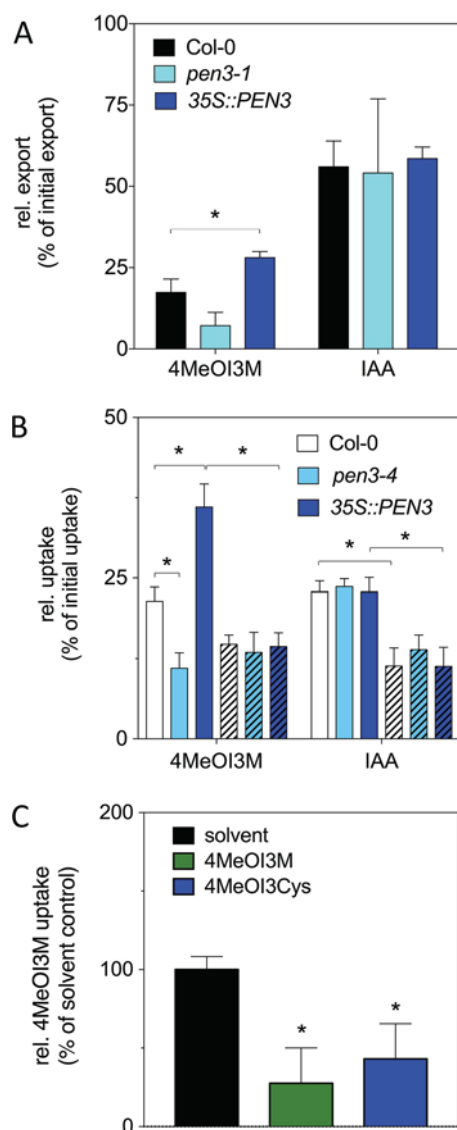
6

Figure 5. 4MeOI3M is transported in a PEN3-dependent manner. *A, PEN3* overexpression enhances [³H]4MeOI3M export from protoplasts. Leaf mesophyll protoplasts isolated from Col-0 (WT), *pen3-1*, and *35S::PEN3* plants were loaded with [³H]4MeOI3M or [¹⁴C]IAA. Export of radioactively labeled compounds was measured by scintillation counting of supernatants. Data are plotted as export relative to initial export. *B, PEN3*-dependent uptake of [³H]4MeOI3M into microsomes. Microsomes isolated from Col-0 (WT), *pen3-4*, and *35S::PEN3* mixotrophic liquid cultures were incubated with [³H]4MeOI3M and [¹⁴C]IAA in the presence (*clear bars*) or absence of ATP (*hatched bars*). After 10 s and 2 min of incubation, samples were harvested, washed, and subjected to scintillation counting. Data are plotted as relative uptake normalized to the initial time point (10 s). *C,* unlabeled 4MeOI3M and 4MeOI3Cys compete with [³H]4MeOI3M microsomal uptake. Microsomes isolated from *35S::PEN3* mixotrophic liquid cultures were incubated with [³H]4MeOI3M in the presence of solvent or a 100-fold excess of unlabeled 3MeOI3M or 4MeOI3Cys. Samples and data handling were performed as in *B.* Combined data of at least four independent experiments with four replicates each are presented. Significance analyses were performed by unpaired *t* tests (*, *p* < 0.05). *Error bars*, S.E.

4MeOI3Cys and 4MeOI3M do not inhibit P. infestans growth

The absence of 4MeOI3M and 4MeOI3Cys on the leaf surface correlates with enhanced penetration of epidermal cells by *P. infestans*. To analyze whether these substances have antimicrobial activity, their impact on *P. infestans* growth was tested *in vitro* inhibition assays using a GFP-expressing *P. infestans* isolate (26) (Fig. 7A). In contrast to known anti-oomycotic

compounds, such as azoxystrobin and γ-oxocrotonate ((2*E*)-4-oxohexadec-2-enoic acid) (27), no significant differences in mycelial growth of *P. infestans* were observed in the presence of 100 μM 4MeOI3M or 4MeOI3Cys, suggesting that these substances do not act as anti-oomycotic compounds at physiological concentrations.

4MeOI3M induces elevations in cytosolic Ca²⁺ levels

The observation that none of the PEN3-dependently exported compounds acted against *P. infestans* at physiological concentrations suggested that they might act as modulators of plant defense. Therefore, elicitation of defense responses by the newly identified compounds were addressed in *Arabidopsis* seedlings.

4MeOI3M was assayed in a luminescence-based Ca²⁺ reporter assay (28, 29). Using aequorin-expressing plants allows to monitor the calcium fluxes, which are the hallmark of early biotic and abiotic stress responses. The addition of 10 μM 4MeOI3M elicited a significant transient increase in cytoplasmic Ca²⁺, albeit lower than that activated by Pep1 (Fig. 7B), suggesting that 4MeOI3M acts as an activator of the Ca²⁺ response. The addition of 4MeOI3CHO did not lead to changes in the Ca²⁺ response. Similarly, neither 4MeOI3Cys nor I3MA elicited an elevation of cytosolic Ca²⁺ concentration (Fig. 7C).

To address possible effects of 4MeOI3M on early receptor-mediated signaling responses, activation of defense-related MAPKs was monitored by Western blotting using an antibody specific for phosphorylated MAPK-pTEpY motifs. In contrast to flg22, the addition of 4MeOI3M to *Arabidopsis* protoplasts did not lead to MAPK activation (Fig. 7D). Because *Arabidopsis* protoplasts did not tolerate higher DMSO concentrations, 4MeOI3Cys could not be tested in this system due to its low water solubility.

Extracellular 4MeOI3M restores flg22-induced callose deposition in pen3-1 seedlings

In addition to enhanced penetration frequencies after inoculation of nonadapted pathogens, *pen* mutants also show defects in callose deposition in response to flg22 treatment (7). To address the question whether extracellular 4MeOI3M can alter this phenotype, Col-0 and *pen3-1* seedlings were treated with flg22 in the presence and absence of 4MeOI3M. Leaves were stained for callose with aniline blue. Microscopic analyses showed callose deposition in WT plants in response to flg22, but not to 4MeOI3M treatment (Fig. 8, *A* and *B*). In *pen3-1* plants, callose deposition in response to flg22 treatment was highly reduced compared with that of flg22-treated WT plants (Fig. 8C). As for Col-0, exogenous application of 4MeOI3M alone did not induce callose deposition in *pen3-1* (Fig. 8D). Treatment of *pen3-1* mutant seedlings with both flg22 and 4MeOI3M resulted in enhanced callose staining (Fig. 8E). Quantification of the staining revealed significantly reduced callose depositions in flg22-treated *pen3-1* compared with Col-0 plants (Fig. 8F). Application of 4MeOI3M to flg22-treated *pen3-1* plants resulted in significantly enhanced callose depositions, albeit not to
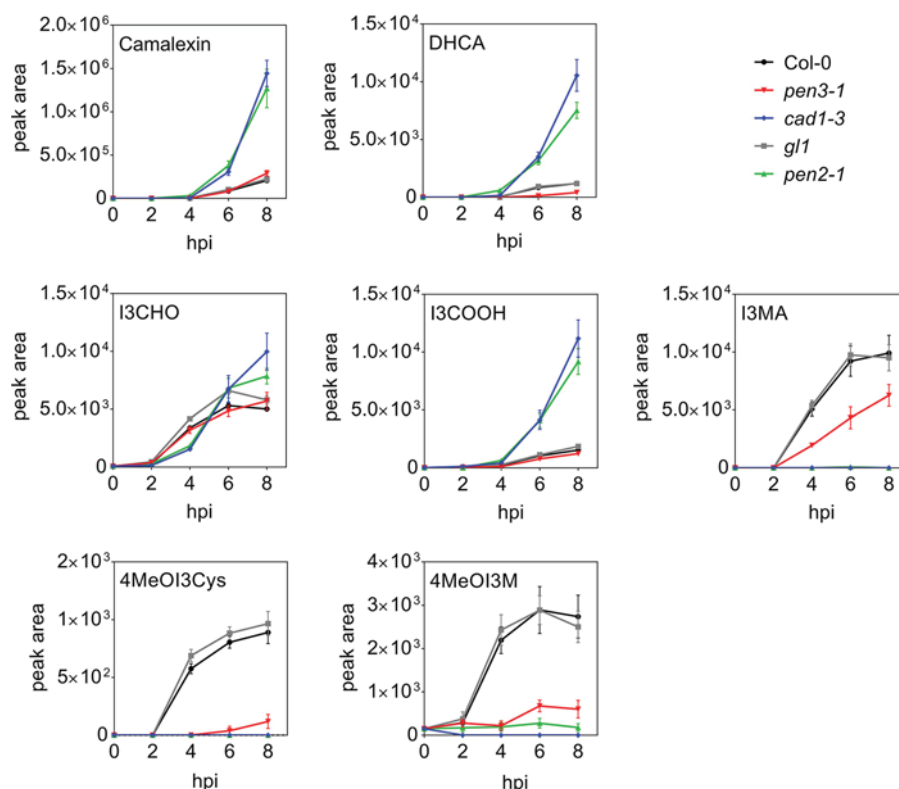
Figure 6. Time course of *P. infestans*-induced extracellular accumulation of metabolites. Leaves of the *Arabidopsis* mutants *pen3-1* (*red*), *cad1-3* (*blue*), and *pen2-1* (*green*), as well as their respective WTs Col-0 (*black*) and *gl1* (*gray*) were drop-inoculated with a *P. infestans* zoospore suspension (5×10^5 spores ml^{-1}). Metabolite levels were determined by UPLC-ESI-QTOF-MS in the inoculum collected at the time points indicated. Data are derived from three independent experiments ($n = 9$). *Error bars*, S.E.

WT levels, suggesting that 4MeOI3M is able to partially rescue the *pen3* phenotype.

Callose depositions were also observed at hydathodes of cotyledons in response to flg22 treatment compared with control treatment. Application of both flg22 and 4MeOI3M resulted in enhanced labeling of callose, as exemplified for Col-0 in Fig. 8*G*. Quantification of the intensity of callose staining revealed that, in response to flg22 and 4MeOI3M co-treatment, all genotypes showed significantly enhanced callose staining compared with flg22 treatment alone (Fig. 8*H*), suggesting that 4MeOI3M enhances flg22-induced callose formation in hydathodes.

Discussion

4MeOI3M and 4MeOI3Cys synthesis requires PEN2 and PCS1

Using untargeted profiling of extracellular metabolites, potential substrates of the PEN3 transporter were identified. Secretion of metabolites into the inoculum of *P. infestans* was first described by Böttcher *et al.* (16), and this subsequently enabled the identification of a MATE transporter required for export of phenylpropanoid defense compounds during the nonhost resistance response of *Arabidopsis* against *P. infestans* (17). Here, 4MeOI3Cys and 4MeOI3M were identified as substances that are synthesized, and exported, in a PEN2- and PCS1- as well as PEN3-dependent manner, respectively. The proposed pathway of synthesis of 4MeOI3Cys and 4MeOI3M postulates the PEN2-mediated catabolism of 4MeOI3G to 4-methoxyindol-3-ylmethyl isothiocyanate. PEN2 hydrolyzes both I3G and 4MeOI3G (6). Increased 4MeOI3G levels are

observed in *P. infestans*-inoculated *pen2-1* mutants, similar to those reported for *Bgh* inoculation (6), suggesting that the loss of conversion results in substrate accumulation. The product of the reaction is converted by yet unidentified enzymes. Recent genetic data suggest the involvement of the GSH-*S*-transferase GSTU13 in the synthesis of PEN2-derived metabolites (12). In accordance with the pathway proposed by these authors, GSH could be attached to 4-methoxyindol-3-ylmethyl isothiocyanate, resulting in the loss of thiocyanate (12). Glycine and glutamic acid would have to be removed from the resulting metabolite by peptidases. We propose that PCS1 is involved in this step, because this enzyme has been shown to catalyze the removal of glycine from GSH conjugates *in vitro* (30) and *in planta* (31). PCS1 catalyzes the formation of phytochelatins, (γ-Glu-Cys)$_n$-Gly, which are required for heavy metal tolerance. In addition to metal hypersensitivity, *pcs1* mutants, such as *cad1-3*, are less responsive to flg22 (7) and display reduced penetration resistance to *P. infestans* (21). These two functions are separate, because cadmium sensitivity, but not the *P. infestans*-induced phenotype of *cad1-3* mutants is rescued by the expression of *Caenorhabditis elegans* PCS. *Ce*PCS is able to synthesize phytochelatins (32) and is, thus, able to restore heavy metal tolerance to *pcs1* mutants (21). The inability of *Ce*PCS1 to rescue the *P. infestans*-related phenotype of *cad1-3* might correlate with the inability to produce extracellular 4MeOI3M und 4MeOI3Cys. Because *Ce*PCS lacks a plant-specific C-terminal domain, it can be speculated that this C-terminal domain is involved in converting plant secondary metabolites. We thus
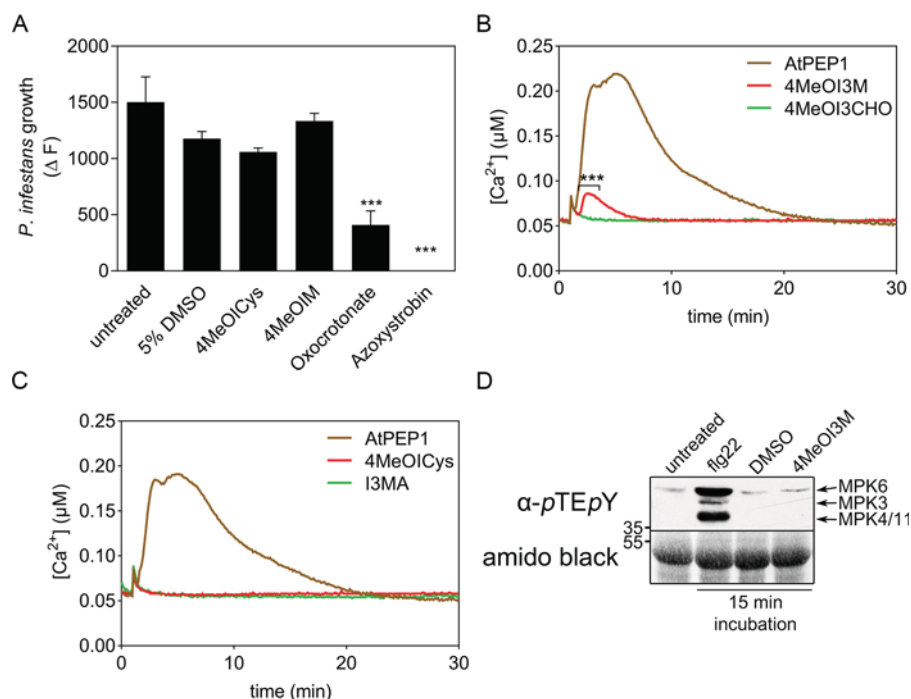
Figure 7. 4MeOI3M induces elevation of cytosolic Ca²⁺ concentrations but does not inhibit *P. infestans* mycelial growth *in vitro*. *A*, 100 μM 4MeOI3M, 4MeOI3Cys, oxocrotonate ((*E*)-4-oxohexadec-2-enoic acid), or azoxystrobin was added to a sporangia suspension (1×10^4 ml^{-1}) of a GFP-expressing *P. infestans* isolate growing *in vitro*. GFP fluorescence was measured daily. Growth was determined by the difference in fluorescence at day 5 compared with day 1, the time point when the compounds were added. Data are derived from three independent experiments ($n = 9$). *Error bars*, S.E. Significance analyses were performed using the Mann–Whitney two-tailed *U* test (compounds *versus* 5% DMSO treatment; *, $p < 0.05$; **, $p < 0.01$; ***, $p < 0.001$). *B* and *C*, 4MeOI3M induces elevation of cytosolic Ca²⁺ concentrations. Apoaequorin-expressing Col-0 seedlings were treated with 10 μM 4MeOI3M, 4MeOI3CHO (*B*), 4MeOI3Cys or I3MA (*C*), or AtPEP1 as a positive control. Data are representative of three independent experiments. Significance analyses were performed by two-way repeated measures analysis of variance (***, $p < 0.001$). *D*, 4MeOI3M does not activate MAPKs. *Arabidopsis* protoplasts were treated with 100 nM flg22, 5% DMSO, or 100 μM 4MeOI3M. Total protein was extracted after 15 min of incubation and subjected to Western blot analysis. Activated MAPKs were detected with an antibody against the phosphorylated pTEpY motif. Amido Black staining was performed to assess loading. Data presented are representative of two independent experiments.

hypothesize that this domain is required for the formation of 4MeOI3Cys.

4MeOI3M is transported in a PEN3-dependent manner

The PEN3-dependent extracellular occurrence of 4MeOI3M und 4MeOI3Cys suggested that these compounds are substrates of the ABC transporter or metabolites of the transported substrate. Using *Arabidopsis* protoplast and microsome transport assays, we were able to demonstrate that 4MeOI3M is transported by PEN3. Like other PDR-type ABC transporters, PEN3 is able to transport several structurally loosely related substrates. However, despite accepting various compounds like IBA and 4MeOI3M, PEN3 still displays a high specificity for these few substrates, which is also reflected by the finding that IBA, but not closely related IAA, is transported by PEN3 (25, 23). A recently identified allele of *pen3*, *pen3-5*, shows differential effects on IBA and pathogen responses (15), providing a molecular rationale for substrate uncoupling.

Interestingly, partial conversion of 4MeOI3Cys into 4MeOI3M was observed *in vitro* (data not shown), suggesting the possibility that metabolism of PEN3-transported 4MeOI3Cys contributes to the overall levels of 4MeOI3M that we detected on the leaf surface of *P. infestans*-inoculated plants.

Based on the overaccumulation of 4GlcOI3F in *Bgh*-inoculated *pen3* leaves, a precursor of this compound was proposed

to be the substrate of PEN3 (15). However, we were unable to detect 4GlcOI3F in methanolic extracts of *P. infestans*-inoculated *pen3-1* leaves, suggesting that different pathogens might induce distinct branches of the PEN2 hydrolytic pathway. Interestingly, in *pen3-1*, loss of PEN3 function does not result in a pronounced accumulation of the transported substrate. In fact, only very low and variable levels of 4MeOI3M and 4MeOI3Cys are detectable in methanolic extracts of *P. infestans*-inoculated leaves. This observation points to the possibility of the formation of a metabolon to achieve metabolite channeling. Metabolon formation has been postulated for enzymes of other secondary metabolites, such as sporopollenin in *Arabidopsis* (33) and soybean isoflavonoids (34). Moreover, the cyanogenic glucoside dhurrin of *Sorghum bicolor* is synthesized by interacting enzymes (35). The efficient formation of this defense compound requires a metabolon consisting of four enzymes and a negatively charged lipid surface (36). In our proposed pathway, 4MeOI3G is catabolized by PEN2, a GSH-*S*-transferase, and a peptidase, as well as by PCS1. Because other intermediates of this postulated pathway were not detectable either, degradation of 4MeOI3G and subsequent formation and export of 4MeOI3Cys and 4MeOI3M might occur in a metabolon, in which cooperating enzymes are brought together (37). Recently, Fuchs *et al.* (14) reported on the close proximity of
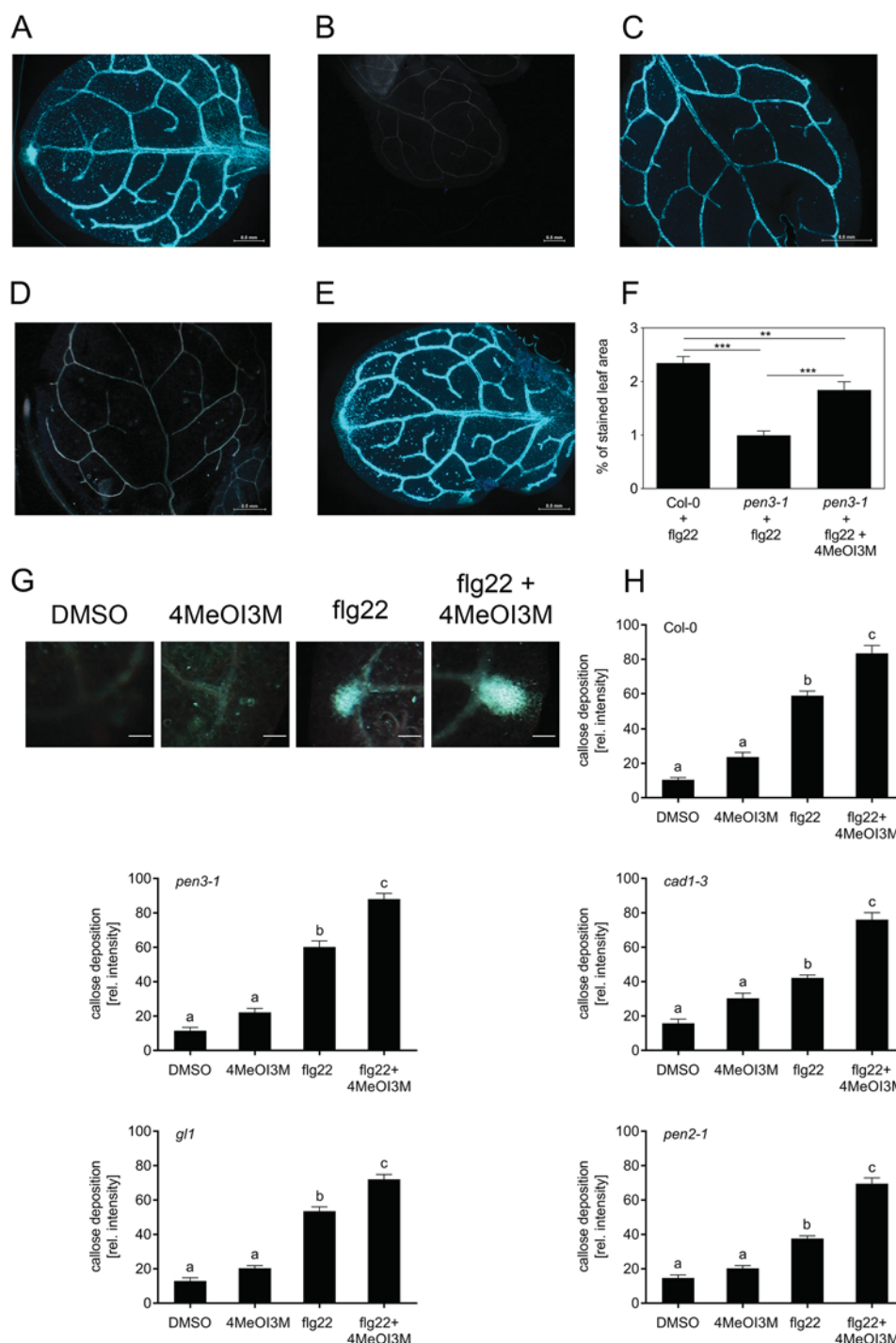
9

Figure 8. 4MeOI3M enhances flg22-induced callose formation. Seedlings growing in liquid culture were treated with 1 μM flg22, 100 μM 4MeOI3M, or 1 μM flg22 and 100 μM 4MeOI3M for 24 h. Callose was stained with aniline blue in Col-0 seedlings treated with flg22 (*A*) or 4MeOI3M (*B*) and in *pen3-1* seedlings treated with flg22 (*C*), 4MeOI3M (*D*), or flg22 and 4MeOI3M (*E*). *F*, quantification of callose depositions in Col-0 and *pen3-1* seedlings. The extent of callose staining was quantified using ImageJ. The percentage of stained area compared with total area was calculated for each leaf; at least 80 individual leaves were analyzed. Significance analyses were performed using the Mann–Whitney two-tailed *U* test (**, $p < 0.01$; ***, $p < 0.001$). *G*, callose formation at hydathodes of cotyledons in Col-0. Eleven-day-old seedlings were incubated with 1% DMSO, 1 μM flg22 in 1% DMSO or 100 μM 4MeOI3M in 1% DMSO or both for 24 h and stained for callose using aniline blue. *Scale bars*, 100 μm. *H* and *I*, quantification of callose depositions at hydathodes of WT and *pen* mutant plants. Intensity of aniline blue staining was determined in microscopic images by determining the mean gray value using ImageJ. Data were obtained in three independent experiments. Significance analyses were performed by two-tailed unpaired *t* test (Col-0: DMSO, $n = 46$; 4MeOI3M, $n = 38$; flg22, $n = 107$, flg22 + 4MeOI3M, $n = 98$; *pen3-1*: DMSO, $n = 31$; 4MeOI3M, $n = 48$; flg22, $n = 93$; flg22 + 4MeOI3M, $n = 127$; *cad1-3*: DMSO, $n = 46$; 4MeOI3M, $n = 38$; flg22, $n = 107$; flg22 + 4MeOI3M, $n = 98$; *gl1*: DMSO, $n = 33$; 4MeOI3M, $n = 63$; flg22, $n = 110$; flg22 + 4MeOI3M, $n = 130$; *pen2-1:* DMSO, $n = 55$; 4MeOI3M, $n = 51$; flg22, $n = 113$; flg22 + 4MeOI3M, $n = 91$). *Error bars*, S.E.

CYP81F2, the enzyme catalyzing the formation of 4OHI3G from I3G, to PEN2 in immobilized mitochondria at the site of attempted penetration of *Bgh*. Thus, formation of a micro-compartment consisting of the different enzymes and of the transporter PEN3 might also be responsible for the efficient production and export of 4MeOI3M und 4MeOI3Cys.

4MeOI3M induces Ca²⁺ transients and enhances flg22-induced callose deposition

The loss of penetration resistance against *P. infestans* in *pen3-1* correlates with highly reduced extracellular levels of 4MeOI3M and 4MeOI3Cys. Possible functions of extracellular metabolites in pathogen resistance include antimicrobial activity or the activation of plant defense. In other pathosystems, the hydrolysis products of 4MeOI3G are considered to contribute to penetration resistance against filamentous pathogens due to antimicrobial activity (6, 8, 14). The inability of 4MeOI3M and 4MeOI3Cys to inhibit mycelial growth of *P. infestans in vitro*, however, does not support a direct antimicrobial effect as the basis for penetration resistance against the oomycete.

Genetic analyses had suggested that 4MeOI3G hydrolysis products are required for flg22-induced callose formation (7). In contrast to chitin, flg22 requires functional *PEN2*, *PCS1*, and *PEN3* genes for the induction of callose depositions (38). The PEN2 substrate 4MeOI3G can restore callose deposition in IG biosynthesis mutants, but not in mutants affected in genes involved in IG hydrolysis, such as *pen2* and *pcs1*, nor in the transport mutant *pen3* (7). Based on these results, a hydrolysis product of 4MeOI3G was postulated to act as a signaling molecule or a potential coactivator of callose formation (7, 38).

The observation that 4MeOI3M induces Ca²⁺ transients could suggest a signaling function for this PEN2/PCS1- and PEN3-dependently synthesized and exported compound. However, because 4MeOI3M does not activate MAPKs, it does not appear to be a general inducer of defense responses. In addition to Ca²⁺ transients, flg22-induced callose deposition is enhanced in the presence of exogenous 4MeOI3M. Mechanistically, a direct effect of 4MeOI3M on callose formation can be envisaged, because early studies report a Ca²⁺ dependence of callose synthases of cultured plant cells (39). Thus, the small, but highly significant, increase in cytosolic Ca²⁺ concentrations induced by exogenous 4MeOI3M might lead to the local activation of a callose synthase.

Stomata and hydathodes are bacterial entry sites and represent a first barrier to pathogen invasion (40). It is interesting to note that both *PEN3* and the flg22 receptor–encoding gene *FLS2* are highest expressed in stomata and hydathodes (41, 42). Our observation that 4MeOI3M contributes to callose formation in hydathodes and, thus, to the structural barrier against bacterial invasion, might therefore indicate a positive role for PEN3 in defense against bacterial pathogens. This is in accordance with data showing reduced callose formation and enhanced susceptibility of *pen3* to *Pseudomonas syringae* pv. *tomato* (43). However, there are also reports of enhanced resistance of *pen3* to *Pst*DC3000 (13, 41). Different bacterial titers and inoculation methods may account for these divergent results. At this point, these data indicate that our knowledge of mechanisms involved in defense at the cell periphery is not advanced enough to explain all observed phenomena. The identification of a 4MeOI3G hydrolysis product, which (i) is synthesized in a PEN2-dependent manner, (ii) is transported by PEN3 *in vitro*, and (iii) contributes to flg22-induced callose formation, adds to our understanding of these early regulatory networks important for proper defense at the cell periphery.

Experimental procedures

Plant growth conditions

Arabidopsis mutants *pen2-1* (5), *pen3-1*, *pen3-3*, and *pen3-4* (8); *cad1-3* (22); and the corresponding WTs *gl1* and Col-0 were grown in a phytochamber at 22 °C with a light/dark cycle of 8/16 h (~120 microeinsteins m⁻² s⁻¹, metal halide lamp HQI®-T, Osram).

Sample preparation for metabolite profiling

Rosette leaves of 5-week-old *A. thaliana* plants were drop-inoculated with a zoospore suspension of *P. infestans* Cra208m2 (26) by applying 10-μl drops onto the adaxial leaf surface (5 × 10⁵ spores ml⁻¹). Drops and the leaf tissue below the inoculation sites were collected separately. Recollected inoculation drops (300 μl) were immediately frozen in liquid nitrogen for storage. For extraction, the frozen drops were thawed and evaporated to dryness. Samples were dissolved in 60 μl of 30% methanol (LC-MS CHROMASOLV® Fluka Analytical) and sonicated for 15 min. Following centrifugation at 19,000 × *g* (4 °C) for 10 min, the residue-free samples were transferred to Qsert Vials (Waters Corp.). Leaf material (~100 mg) was frozen in liquid nitrogen. Methanolic extracts were prepared as described (16, 17).

LC/MS measurements

Untargeted metabolite profiling was performed as described (16, 17) with the following modifications. The binary gradient was applied at a flow rate of 150 μl/min with 0–1 min, isocratic 95% A (water/formic acid, 99.9:0.1 (v/v)), 5% B (acetonitrile/formic acid, 99.9:0.1 (v/v)); 1–5 min, linear from 5 to 25% B; 5–10 min, linear to 95% B; 10–12 min, isocratic 95% B; 12–15 min, isocratic 5% B.

Eluting compounds were detected from *m/z* 80 to 1000 using a micrOTOF-Q II hybrid quadrupole TOF mass spectrometer (Bruker Daltonics) equipped with an Apollo II electrospray ion source in positive and negative-ion mode using the following instrument settings: nebulizer gas, nitrogen, 1.4 bar; dry gas, nitrogen, 6 liters/min, 190 °C; capillary, −5000 V; end plate offset, −500 V; funnel 1 RF, 200 V; funnel 2 RF, 200 V; in-source CID energy, 0 V; hexapole RF, 100 V; quadrupole ion energy, 5 eV; collision gas, nitrogen; collision energy, 7 eV; collision RF 150/350 V (timing 50/50); transfer time, 70 μs; prepulse storage, 5 μs; pulser frequency, 10 kHz; spectra rate, 3 Hz. Mass spectra were acquired in centroid mode. Mass calibration of individual raw data files was performed on lithium formate cluster ions obtained by automatic infusion of 20 μl of 10 mM lithium hydroxide in isopropyl alcohol/water/formic acid, 49.9:49.9:0.2 (v/v/v) at a gradient time of 12 min using a diverter valve.

Raw data files were converted to mzData format using the vendor-specific software CompassXport and processed using the XCMS package (http://bioconductor.org/packages/release/bioc/html/xcms.html)[4] (52). XCMS settings for processing LC/MS data with findPeaks.centWave were as follows: prefilter = (3, 200); snthr = 5; ppm = 25; peak width = (5, 12); scan range (50, 1020). For alignment, group density function with parameters minfrac = 0.75 and bw = 5, mzwid = 0.05, max = 20 was used.

---

[4] Please note that the JBC is not responsible for the long-term archiving and maintenance of this site or any other third party hosted site.

Differentially accumulating compounds were determined using Student's t test with $p < 0.05$ and a -fold change of ≥ 2. Each mutant-WT comparison was performed at least four times in independent experimental repetitions with five biological replicates in each experiment (for *pen3-1*, *pen3-3*, and *pen3-4* also using MetaboScape 3.0 Service Release 1 (T-ReX® 3D algorithm (Bruker) with the following settings: peak detection: intensity threshold 1000 counts, minimum peak length 7 spectra, feature signal = intensity; recursive feature extraction: minimum peak length (recursive) 3 spectra. Differentially accumulated features between the lines and treatments were detected with Student's t test or with Welch's t test if equal variances could not be assumed, with missing value substitution with the lowest-intensity value in the whole data set.

Identification of the compounds was based on manual interpretation of MS/MS spectra. For comparison with different mass spectra databases, the open source metabolite identification software MetFrag was used.

Additional LC-MS measurements for targeted metabolite analysis were performed on a micrOTOF-Q quadrupole TOF mass spectrometer (Bruker Daltonics) in positive mode with the same setup as above. Targeted relative quantification of metabolites was performed using peak areas of extracted ion chromatograms in Bruker's QuantAnalysis software. Figures were created with MetaboScape 3.0 Service Release 1 (Bruker) and with GraphPad Prism 7.04.

Synthesis of 4MeOI3M and 4MeOI3Cys

Column chromatography was performed on silica gel 60 (Merck, $40-63$-μm particle size) and Sephadex LH 20 (Fluka) using cylindrical glass columns with glass frits or plugged with cotton wool, whereas analytical TLC was performed on precoated silica gel F254 plates (Merck). The compound spots were detected by their UV absorbance at λ 254 nm and/or by spraying of the TLC plates with vanillin-sulfuric acid reagent followed by heating in a hot air stream. One-dimensional (^{1}H, ^{13}C) NMR spectra were obtained from an Agilent DD2 400 system. The spectra were recorded at 400 MHz (^{1}H) and 100 MHz (^{13}C), respectively. Chemical shifts were referenced to internal TMS (δH 0, ^{1}H) or CDCl3 (δC 77.0, ^{13}C).

The positive-ion high-resolution ESI mass spectra were obtained from an Orbitrap Elite mass spectrometer (Thermo Fisher Scientific) equipped with an HESI electrospray ion source (spray voltage 3.5 kV, capillary temperature 275 °C, source heater temperature 40 °C, Fourier transform MS resolution 60,000). Nitrogen was used as sheath gas. The sample solutions were introduced continuously via a 500-μl Hamilton syringe pump with a flow rate of 5 μl min^{-1}. The instrument was externally calibrated by the Pierce LTQ Velos ESI calibration solution from Thermo Fisher Scientific. The data were evaluated by the Xcalibur software 2.7 SP1 (Thermo Fisher Scientific).

4-Methoxyindol-3-yl methanol (44) was synthesized by the addition of 4-methoxy-indole-3-carbaldehyde (2.80 g, 16.0 mmol) to 50 ml of a solvent mixture consisting of methanol/ethanol/chloroform (1:8:5, v/v/v), upon which NaBH$_4$ (0.60 g, 16.0 mmol) was added at room temperature. After stirring for 6 h, the solvent was removed under reduced pressure, and

NaOH (28 ml, 0.1 M) was added to the residue. Upon extraction with diethyl ether (3×60 ml), the combined organic extracts were dried over Na$_2$SO$_4$, filtered, and evaporated. The remaining light brown oil was purified by chromatography on silica gel (methylene chloride/methanol, 95:5) to yield 1.9 g (67%) of pale yellow oily product. The analytical data were identical to the reported data (44).

For synthesis of *S*-((4-methoxy-1*H*-indol-3-yl)methyl) cysteine (45), a solution of L-cysteine (0.87 g, 7.2 mmol) in water (200 ml) was brought to pH 13 by titration with NaOH (10 N), upon which 4MeOI3M (0.64 g, 3.6 mmol) was added at room temperature under vigorous stirring. Stirring was continued for 12 h at 60 °C. After cooling, the solids were filtered off. The remaining solution was neutralized (pH 7) with HCl (0.2 N), and the precipitate formed was again filtered off and carefully washed with ice-cold water. After drying *in vacuo*, a colorless powder (553 mg, 56%) remained.

TLC $R_f = 0.81$ (ethyl acetate/ethanol/water, 70:15:8). ^{1}H NMR (400 MHz, CD$_3$OD): $\delta = 7.13$ (s, 1H, H-2), $6.98-7.02$ (m, 1H), 6.93 (d, $J = 7.9$ Hz, 1H), 6.46 (d, $J = 7.45$ Hz, 1H,), 4.11 (d, $J = 13.6$ Hz, 2H, H-3′), 3.89 (s, 3H, CH$_3$), 3.68 (dd, $J = 4.0, 9.2$ Hz, 1H, H-1), 3.14 (dd, $J = 4.0, 14.4$ Hz, 1H, H2a), 2.83 (dd, $J = 8.8, 14.5$ Hz, 1H, H2b). ^{13}C NMR (100 MHz, DMSO-d_6): $\delta = 168.8, 154.3, 138.0, 123,1, 122.1, 116.2, 110.9, 105.0, 99.2, 55.1, 53.5, 32.1, 27.4$. ESI-MS m/z: 281.2 [M + H]$^+$, 303.2 [M + Na]$^+$. [^{3}H]4MeOI3M, labeled at the aromatic core, was provided by Hartmann Analytics.

PEN3 transport experiments

Intact *Arabidopsis* mesophyll protoplasts from Col-0 (WT), *pen3-4*, and *35S::PEN3* were prepared from rosette leaves of plants grown on soil under a 100-μmol m^{-2} s^{-1} white light, 8-h light/16-h dark cycle at 22 °C as described (46). Protoplasts were loaded by incubation with 1 μl ml^{-1} of a mixture of [^{3}H]4MeOI3M (custom-synthesized by Hartman Analytics, specific activity 5.7 Ci/mmol) and [^{14}C]IAA (specific activity 55 Ci mmol^{-1}; American Radiolabeled Chemicals). External radioactivity was removed by separating protoplasts using a $50-30$-5% Percoll gradient. Transport was initiated by incubation at 25 °C and halted by silicon oil centrifugation. Effluxed radioactivity was determined by scintillation counting of aqueous phases and is presented as the relative efflux of the initial efflux (efflux prior to temperature incubation), which was set to zero.

For microsomal uptake experiments, Col-0 (WT), *pen3-4*, and *35S::PEN3* total microsomes were prepared from mixotrophic liquid cultures as described elsewhere (46). Combinations of labeled [^{3}H]4MeOI3M and [^{14}C]IAA, respectively, were diluted into transport buffer (10 mM Tris-HCl, 10 mM MgCl$_2$, 1 mM EDTA, 1 mM DTT, 10% sucrose, pH 7.6, with 5 mM ATP) and added to 300 μg of microsomes to yield a final concentration of 1 μM each. After 10 s and 2 min of incubation at 20 °C, four aliquots of 100 μl were vacuum-filtered on Whatman NC45 filters (GE Healthcare) and washed three times with 1 ml of cold double-distilled H$_2$O. Air-dried filters were subjected to scintillation counting. Indicated relative uptake was calculated as the radioactivity normalized to the first time point (10 s). For substrate competition assays, unlabeled substrate

was included in the transport buffer at a 100-fold excess. Means and S.E. values of at least four independent experiments with four technical replicates each are presented.

P. infestans inhibition assays

Mycelial growth inhibition assays were performed with *P. infestans* Cra208m2 (26) as described (27, 47).

Ca²⁺ and MAPK assays

Col-0 plants expressing cytosolic *p35S:Apoaequorin* were used for aequorin luminescence-based Ca^{2+} measurements (pMAQ2; 28). Ca^{2+} measurements, protoplast transformation, and MAPK assays were performed as described (29).

Callose staining of hydathodes

Eleven-day-old seedlings grown in microtiter plates were treated with 1% DMSO, 1 μM flg22 in 1% DMSO or 100 μM 4MeOI3M in 1% DMSO for 24 h. Staining of callose with aniline blue was performed as described (7, 48). Quantification was performed using the image processing package Fiji (ImageJ) (49) for primary leaves as described (50). Intensity of callose staining in hydathodes was determined as the mean gray value in photographs taken with identical settings.

Accession numbers

Sequence data from this article can be found in the Arabidopsis Genome Initiative or GenBank™/EMBL databases under the following accession numbers: At2g44490 (*PEN2*), At5g44070 (*PCS1*), and At1g59870 (*PEN3*).

References

1. Kamoun, S. (2001) Nonhost resistance to *Phytophthora*: novel prospects for a classical problem. *Curr. Opin. Plant Biol.* **4,** 295–300 CrossRef Medline
2. Fan, J., and Doerner, P. (2012) Genetic and molecular basis of nonhost disease resistance: complex, yes; silver bullet, no. *Curr. Opin. Plant Biol.* **15,** 400–406 CrossRef Medline
3. Stam, R., Mantelin, S., McLellan, H., and Thilliez, G. (2014) The role of effectors in nonhost resistance to filamentous plant pathogens. *Front. Plant Sci.* **5,** 582 CrossRef Medline
4. Schulze-Lefert, P., and Panstruga, R. (2011) A molecular evolutionary concept connecting nonhost resistance, pathogen host range, and pathogen speciation. *Trends Plant Sci.* **16,** 117–125 CrossRef Medline
5. Lipka, V., Dittgen, J., Bednarek, P., Bhat, R., Wiermer, M., Stein, M., Landtag, J., Brandt, W., Rosahl, S., Scheel, D., Llorente, F., Molina, A., Parker, J., Somerville, S., and Schulze-Lefert, P. (2005) Pre- and postinvasion defenses both contribute to nonhost resistance in *Arabidopsis. Science* **310,** 1180–1183 CrossRef Medline
6. Bednarek, P., Pislewska-Bednarek, M., Svatos, A., Schneider, B., Doubsky, J., Mansurova, M., Humphry, M., Consonni, C., Panstruga, R., Sanchez-Vallet, A., Molina, A., and Schulze-Lefert, P. (2009) A glucosinolate metabolism pathway in living plant cells mediates broad-spectrum antifungal defense. *Science* **323,** 101–106 CrossRef Medline
7. Clay, N. K., Adio, A. M., Denoux, C., Jander, G., and Ausubel, F. M. (2009) Glucosinolate metabolites required for an *Arabidopsis* innate immune response. *Science* **323,** 95–101 CrossRef Medline
8. Stein, M., Dittgen, J., Sánchez-Rodriguez, C., Hou, B. H., Molina, A., Schulze-Lefert, P., Lipka, V., and Somerville, S. (2006) Arabidopsis PEN3/PDR8, an ATP binding cassette transporter, contributes to nonhost resistance to inappropriate pathogens that enter by direct penetration. *Plant Cell* **18,** 731–746 CrossRef Medline
9. Westphal, L., Scheel, D., and Rosahl, S. (2008) The coi1–16 mutant harbors a second site mutation rendering PEN2 nonfunctional. *Plant Cell* **20,** 824–826 CrossRef Medline
10. Halkier, B. A., and Gershenzon, J. (2006) Biology and biochemistry of glucosinolates. *Annu. Rev. Plant Biol.* **57,** 303–333 CrossRef Medline
11. Pfalz, M., Mikkelsen, M. D., Bednarek, P., Olsen, C. E., Halkier, B. A., and Kroymann, J. (2011) Metabolic engineering in *Nicotiana benthamiana* reveals key enzyme functions in *Arabidopsis* indole glucosinolate modification. *Plant Cell* **23,** 716–729 CrossRef Medline
12. Piślewska-Bednarek, M., Nakano, R. T., Hiruma, K., Pastorczyk, M., Sanchez-Vallet, A., Singkaravanit-Ogawa, S., Ciesiołka, D., Takano, Y., Molina, A., Schulze-Lefert, P., and Bednarek, P. (2018) Glutathione transferase U13 functions in pathogen-triggered glucosinolate metabolism. *Plant Physiol.* **176,** 538–551 CrossRef Medline
13. Johansson, O. N., Fantozzi, E., Fahlberg, P., Nilsson, A. K., Buhot, N., Tör, M., and Andersson, M. X. (2014) Role of the penetration-resistance genes *PEN1, PEN2* and *PEN3* in the hypersensitive response and race-specific resistance in *Arabidopsis thaliana. Plant J.* **79,** 466–476 Medline
14. Fuchs, R., Kopischke, M., Klapprodt, C., Hause, G., Meyer, A. J., Schwarzländer, M., Fricker, M. D., and Lipka, V. (2016) Immobilized subpopulations of leaf epidermal mitochondria mediate PENETRATION2-dependent pathogen entry control in *Arabidopsis. Plant Cell* **28,** 130–145 CrossRef Medline
15. Lu, X., Dittgen, J., Piślewska-Bednarek, M., Molina, A., Schneider, B., Svatoš, A., Doubský, J., Schneeberger, K., Weigel, D., Bednarek, P., and Schulze-Lefert, P. (2015) Mutant allele-specific uncoupling of PENETRATION3 functions reveals engagement of the ATP-binding cassette transporter in dstinct tryptophan metabolic pathways. *Plant Physiol.* **168,** 814–827 CrossRef Medline
16. Böttcher, C., Westphal, L., Schmotz, C., Prade, E., Scheel, D., and Glawischnig, E. (2009) The multifunctional enzyme CYP71B15 (PHYTOALEXIN DEFICIENT3) converts cysteine-indole-3-acetonitrile to camalexin in the indole-3-acetonitrile metabolic network of *Arabidopsis thaliana. Plant Cell* **21,** 1830–1845 CrossRef Medline
17. Dobritzsch, M., Lübken, T., Eschen-Lippold, L., Gorzolka, K., Blum, E., Matern, A., Marillonnet, S., Böttcher, C., Dräger, B., and Rosahl, S. (2016) MATE transporter-dependent export of hydroxycinnamic acid amides. *Plant Cell* **28,** 583–596 CrossRef Medline
18. Böttcher, C., Chapman, A., Fellermeier, F., Choudhary, M., Scheel, D., and Glawischnig, E. (2014) The biosynthetic pathway of indole-3-carbaldehyde and indole-3-carboxylic acid derivatives in *Arabidopsis. Plant Physiol.* **165,** 841–853 CrossRef Medline
19. Rajniak, J., Barco, B., Clay, N. K., and Sattely, E. S. (2015) A new cyanogenic metabolite in *Arabidopsis* required for inducible pathogen defence. *Nature* **525,** 376–379 CrossRef Medline
20. Nafisi, M., Goregaoker, S., Botanga, C. J., Glawischnig, E., Olsen, C. E., Halkier, B. A., and Glazebrook, J. (2007) *Arabidopsis* cytochrome P450 monooxygenase 71A13 catalyzes the conversion of indole-3-acetaldoxime in camalexin synthesis. *Plant Cell* **19,** 2039–2052 CrossRef Medline
21. Kühnlenz, T., Westphal, L., Schmidt, H., Scheel, D., and Clemens, S. (2015) Expression of *Caenorhabditis elegans* PCS in the *AtPCS1*-deficient *Arabidopsis thaliana cad1-3* mutant separates the metal tolerance and non-host resistance functions of phytochelatin synthases. *Plant Cell Environ.* **38,** 2239–2247 CrossRef Medline

22. Howden, R., Goldsbrough, P. B., Andersen, C. R., and Cobbett, C. S. (1995) Cadmium-sensitive, cad1 mutants of *Arabidopsis thaliana* are phytochelatin deficient. *Plant Physiol.* **107,** 1059–1066 CrossRef Medline

23. Ruzicka, K., Strader, L. C., Bailly, A., Yang, H., Blakeslee, J., Langowski, L., Nejedlá, E., Fujita, H., Itoh, H., Syono, K., Hejátko, J., Gray, W. M., Martinoia, E., Geisler, M., Bartel, B., *et al.* (2010) *Arabidopsis* PIS1 encodes the ABCG37 transporter of auxinic compounds including the auxin precursor indole-3-butyric acid. *Proc. Natl. Acad. Sci. U.S.A.* **107,** 10749–10753 CrossRef Medline

24. Kim, D. Y., Bovet, L., Maeshima, M., Martinoia, E., and Lee, Y. (2007) The ABC transporter AtPDR8 is a cadmium extrusion pump conferring heavy metal resistance. *Plant J.* **50,** 207–218 CrossRef Medline

25. Strader, L. C., and Bartel, B. (2009) The *Arabidopsis* PLEIOTROPIC DRUG RESISTANCE8/ABCG36 ATP binding cassette transporter modulates sensitivity to the auxin precursor indole-3-butyric acid. *Plant Cell* **21,** 1992–2007 CrossRef Medline

26. Si-Ammour, A., Mauch-Mani, B., and Mauch, F. (2003) Quantification of induced resistance against *Phytophthora* species expressing GFP as a vital marker: β-aminobutyric acid but not BTH protects potato and *Arabidopsis* from infection. *Mol. Plant Pathol.* **4,** 237–248 CrossRef Medline

27. Eschen-Lippold, L., Draeger, T., Teichert, A., Wessjohann, L., Westermann, B., Rosahl, S., and Arnold, N. (2009) Anti-oomycete activity of γ-oxocrotonate fatty acids against *P. infestans*. *J. Agric. Food Chem.* **57,** 9607–9612 CrossRef Medline

28. Knight, M. R., Campbell, A. K., Smith, S. M., and Trewavas, A. J. (1991) Transgenic plant aequorin reports the effects of touch and cold-shock and elicitors on cytoplasmic calcium. *Nature* **352,** 524–526 CrossRef Medline

29. Ranf, S., Eschen-Lippold, L., Pecher, P., Lee, J., and Scheel, D. (2011) Interplay between calcium signalling and early signalling elements during defence responses to microbe- or damage-associated molecular patterns. *Plant J.* **68,** 100–113 CrossRef Medline

30. Beck, A., Lendzian, K., Oven, M., Christmann, A., and Grill, E. (2003) Phytochelatin synthase catalyzes key step in turnover of glutathione conjugates. *Phytochemistry* **62,** 423–431 CrossRef Medline

31. Blum, R., Beck, A., Korte, A., Stengel, A., Letzel, T., Lendzian, K., and Grill, E. (2007) Function of phytochelatin synthase in catabolism of glutathione-conjugates. *Plant J.* **49,** 740–749 CrossRef Medline

32. Clemens, S., Schroeder, J. I., and Degenkolb, T. (2001) *Caenorhabditis elegans* expresses a functional phytochelatin synthase. *Eur. J. Biochem.* **268,** 3640–3643 CrossRef Medline

33. Lallemand, B., Erhardt, M., Heitz, T., and Legrand, M. (2013) Sporopollenin biosynthetic enzymes interact and constitute a metabolon localized to the endoplasmic reticulum of tapetum cells. *Plant Physiol.* **162,** 616–625 CrossRef Medline

34. Dastmalchi, M., Bernards, M. A., and Dhaubhadel, S. (2016) Twin anchors of the soybean isoflavonoid metabolon: evidence for tethering of the complex to the endoplasmic reticulum by IFS and C4H. *Plant J.* **85,** 689–706 CrossRef Medline

35. Nielsen, K. A., Tattersall, D. B., Jones, P. R., and Møller, B. L. (2008) Metabolon formation in dhurrin biosynthesis. *Phytochemistry* **69,** 88–98 CrossRef Medline

36. Laursen, T., Borch, J., Knudsen, C., Bavishi, K., Torta, F., Martens, H. J., Silvestro, D., Hatzakis, N. S., Wenk, M. R., Dafforn, T. R., Olsen, C. E., Motawia, M. S., Hamberger, B., Møller, B. L., and Bassard, J. E. (2016) Characterization of a dynamic metabolon producing the defense compound dhurrin in sorghum. *Science* **354,** 890–893 CrossRef Medline

37. Sweetlove, L. J., and Fernie, A. R. (2013) The spatial organization of metabolism within the plant cell. *Annu. Rev. Plant Biol.* **64,** 723–746 CrossRef Medline

38. Luna, E., Pastor, V., Robert, J., Flors, V., Mauch-Mani, B., and Ton, J. (2011) Callose deposition: a multifaceted plant defense response. *Mol. Plant Microbe Interact.* **24,** 183–193 CrossRef Medline

39. Waldmann, T., Jeblick, W., and Kauss, H. (1988) Induced net Ca^{2+} uptake and callose biosynthesis in suspension-cultured plant cells. *Planta* **173,** 88–95 CrossRef Medline

40. Cerutti, A., Jauneau, A., Auriac, M. C., Lauber, E., Martinez, Y., Chiarenza, S., Leonhardt, N., Berthomé, R., and Noël, L. D. (2017) Immunity at cauliflower hydathodes controls systemic infection by *Xanthomonas campestris* pv campestris. *Plant Physiol.* **174,** 700–716 CrossRef Medline

41. Kobae, Y., Sekino, T., Yoshioka, H., Nakagawa, T., Martinoia, E., and Maeshima, M. (2006) Loss of AtPDR8, a plasma membrane ABC transporter of *Arabidopsis thaliana*, causes hypersensitive cell death upon pathogen infection. *Plant Cell Physiol.* **47,** 309–318 CrossRef Medline

42. Beck, M., Wyrsch, I., Strutt, J., Wimalasekera, R., Webb, A., Boller, T., and Robatzek, S. (2014) Expression patterns of flagellin sensing 2 map to bacterial entry sites in plant shoots and roots. *J. Exp. Bot.* **65,** 6487–6498 CrossRef Medline

43. Xin, X. F., Nomura, K., Underwood, W., and He, S. Y. (2013) Induction and suppression of PEN3 focal accumulation during *Pseudomonas syringae* pv. tomato DC3000 infection of *Arabidopsis*. *Mol. Plant Microbe Interact.* **26,** 861–867 CrossRef Medline

44. Kronbak, R., Duus, F., and Vang, O. (2010) Effect of 4-methoxyindole-3-carbinol on the proliferation of colon cancer cells *in vitro*, when treated alone or in combination with indole-3-carbinol. *J. Agric. Food Chem.* **58,** 8453–8459 CrossRef Medline

45. Ruangyuttikarn, W., Skiles, G. L., and Yost, G. S. (1992) Identification of a cysteinyl adduct of oxidized 3-methylindole from goat lung and human liver microsomal proteins. *Chem. Res. Toxicol.* **5,** 713–719 CrossRef Medline

46. Henrichs, S., Wang, B., Fukao, Y., Zhu, J., Charrier, L., Bailly, A., Oehring, S. C., Linnert, M., Weiwad, M., Endler, A., Nanni, P., Pollmann, S., Mancuso, S., Schulz, A., and Geisler, M. (2012) Regulation of ABCB1/PGP1-catalysed auxin transport by linker phosphorylation. *EMBO J.* **31,** 2965–2980 CrossRef Medline

47. Prost, I., Dhondt, S., Rothe, G., Vicente, J., Rodriguez, M. J., Kift, N., Carbonne, F., Griffiths, G., Esquerré-Tugayé, M. T., Rosahl, S., Castresana, C., Hamberg, M., and Fournier, J. (2005) Evaluation of the antimicrobial activities of plant oxylipins supports their involvement in defense against pathogens. *Plant Physiol.* **139,** 1902–1913 CrossRef Medline

48. Adam, L., and Somerville, S. C. (1996) Genetic characterization of five powdery mildew disease resistance loci in *Arabidopsis thaliana*. *Plant J.* **9,** 341–356 CrossRef Medline

49. Schindelin, J., Arganda-Carreras, I., Frise, E., Kaynig, V., Longair, M., Pietzsch, T., Preibisch, S., Rueden, C., Saalfeld, S., Schmid, B., Tinevez, J. Y., White, D. J., Hartenstein, V., Eliceiri, K., Tomancak, P., and Cardona, A. (2012) Fiji: an open-source platform for biological-image analysis. *Nat. Methods* **9,** 676–682 CrossRef Medline

50. Albert, I., Böhm, H., Albert, M., Feiler, C. E., Imkampe, J., Wallmeroth, N., Brancato, C., Raaymakers, T. M., Oome, S., Zhang, H., Krol, E., Grefen, C., Gust, A. A., Chai, J., Hedrich, R., Van den Ackerveken, G., and Nürnberger, T. (2015) An RLP23-SOBIR-BAK1 complex mediates NLP-triggered immunity. *Nat. Plants* **1,** 15140 CrossRef Medline

51. Sumner, L. W., Amberg, A., Barrett, D., Beale, M. H., Beger, R., Daykin, C. A., Fan, T. W., Fiehn, O., Goodacre, R., Griffin, J. L., Hankemeier, T., Hardy, N., Harnly, J., Higashi, R., Kopka, J., *et al.* (2007) Proposed minimum reporting standards for chemical analysis. *Metabolomics* **3,** 211–221 CrossRef Medline

52. Smith, C. A., Want, E. J., O'Maille, G., Abagyan, R., and Siuzdak, G. (2006) XCMS: processing mass spectrometry data for metabolite profiling using nonlinear peak alignment, matching and identification. *Anal. Chem.* **78,** 779–787 CrossRef Medline

A substrate of the ABC transporter PEN3 stimulates bacterial flagellin (flg22)-induced callose deposition in *Arabidopsis thaliana*

Andreas Matern, Christoph Böttcher, Lennart Eschen-Lippold, Bernhard Westermann, Ulrike Smolka, Stefanie Döll, Fabian Trempel, Bibek Aryal, Dierk Scheel, Markus Geisler and Sabine Rosahl

---

http://doc.rero.ch